KSCE Journal of Civil Engineering (2024) 28(9):3791-3804
DOI 10.1007/s12205-024-0895-9

pISSN 1226-7988, eISSN 1976-3808
www.springer.com/12205

Structural Engineering

Enhancing Durability of Concrete in Saline Soil with Nano-$CaCO_3$ Modification: Investigation and Reliability Analysis

Bo Yang[a], **Xiaopeng Hu**[a], **and Hongxia Qiao**[b]

[a]*School of Civil Engineering, Xi'an University of Architecture and Technology, Xi'an 710055, China*
[b]*School of Civil Engineering, Lanzhou University of Technology, Lanzhou 730050, China*

ARTICLE HISTORY

Received 2 May 2023
Revised 9 January 2024
Accepted 7 April 2024
Published Online 6 June 2024

KEYWORDS

Concrete
Nano-$CaCO_3$
Sulfate attack
Durability
Bivariate wiener process

ABSTRACT

In this study, the effect of nano-$CaCO_3$ on the durability of concrete was investigated by simulating the attack of semi-buried concrete structures in saline soil. Different nano-$CaCO_3$ contents were used to enhance the durability of concrete. The durability of different areas of nano-$CaCO_3$ modified concrete, partially exposed to sulfate solution, was evaluated, and a reliability analysis was conducted. The results indicated that appropriate nano-$CaCO_3$ content can improve the durability of concrete. In this study, concrete with a nano-$CaCO_3$ content of 1% exhibited the highest durability. The corrosion degrees of different areas of the nano-$CaCO_3$ modified concrete partially exposed to the sulfate solution decreased in the following order: dry–wet transition areas (M area) > fully immersed areas (D area) > exposed air areas (T area). A sulfate chemical attack occurred inside the concrete in the dry–wet transition areas, while a sulfate physical attack occurred on the surface concrete. The predicted values of the model agreed well with the test results. The bivariate Wiener process can effectively describe the whole process of performance deterioration of nano-$CaCO_3$ modified concrete.

1. Introduction

Western China has numerous saline soil areas, and the area of the saline soil distribution is growing because of drought and low rainfall (QISL, 2015; Chang et al., 2021). The presence of SO_4^{2-}, Mg^{2+}, CO_3^{2-}, Cl^-, and other ions in saline soil results in the corrosion of concrete. Over time, the concrete in the area has gradually deteriorated, significantly reducing its service life (Zheng, 2010; Zhou et al., 2011). Research has indicated that typical concrete in this region is likely to be severely destroyed owing to corrosion within 1 – 3 years (Yu et al., 2013). Currently, in western China, it is imperative to improve the corrosion resistance of concrete in saline soil areas and extend the service life of the concrete.

Nano-$CaCO_3$ has the advantages of small particle size and large specific surface area, along with physical and chemical properties different from those of traditional materials (Rong et al., 2015; Mehairi and Husein, 2020). Compared with other nano-materials, nano-$CaCO_3$ has the advantages of a low price and high efficiency (Ding et al., 2020) and has been widely used in the plastic (Liang, 2007) and rubber industries (Roy et al., 2019). In recent years, many scholars in the field of construction engineering have conducted a lot of studies on the properties of nano-$CaCO_3$ modified cement-based. In terms of cement hydration, nano-$CaCO_3$ accelerates cement hydration by functioning as a nucleating matrix for hydrated calcium silicate (Pavan Kumar et al., 2021). Additionally, nano-$CaCO_3$ has been demonstrated to shorten the time for C_3S hydration to begin (Sato and Diallo, 2010), to react chemically with C_3A (Sato and Beaudoin, 2011), accelerating the early hydration of concrete and improving the early setting strength of concrete (Kawashima et al., 2013; Yeşilmen et al., 2015). Nano-$CaCO_3$ has a filling effect in concrete, reduces the concrete porosity, optimizes the pore-size distribution, and significantly increases the early compressive strength (Wu et al., 2016; Li et al., 2020). In terms of modifying the properties of concrete, Uthaman et al. (2019) found that found that nano-$CaCO_3$ effectively blocked pores in the concrete and hindered the diffusion and movement of Cl^- to the rebar surface. After optimizing the nano-$CaCO_3$ modified concrete mixture proportions using an orthogonal test, Sun et al. (2020) found that the chloride diffusion coefficient of the concrete was reduced by 40.12% with the addition of nano-$CaCO_3$ and fly ash. However, excessive amounts of nano-$CaCO_3$ can degrade the properties of concrete (Camiletti et al.,

CORRESPONDENCE Bo Yang yangbo0539@163.com School of Civil Engineering, Xi'an University of Architecture and Technology, Xi'an 710055, China

2013; Wu et al., 2016; Li et al., 2020).

Concrete corrosion in foundations, bridge piers, dams, tunnels, and other construction service environments presents significant challenges. Corrosion usually occurs in dry–wet transition areas in these structures. Compared with a fully buried structure, the structure of a semi-buried degree of corrosion is higher (Suleiman et al., 2014; Bassuoni and Rahman, 2016). Chen et al. (2017) indicated that cement mortar specimens partially exposed to a sulfate solution deteriorated in different ways. The upper part of the specimen was subjected to a sulfate physical attack and sulfate chemical attack, while the lower part was subjected to a sulfate chemical attack only. Liu et al. (2012) measured the sulfate concentration and pH of the pore solution in different areas of partially exposed concrete. The results indicated that the sulfate concentration in the pore solution in the upper part of the specimen was significantly higher than that in the lower part. In conclusion, partial exposure test methods are more suitable for simulating the erosion process of concrete structures buried in saline soil.

In the present study, five types of concrete with different nano-$CaCO_3$ contents were prepared. Four durability evaluation parameters were used to reflect the durability deterioration law of different areas of nano-$CaCO_3$ modified concrete partially exposed to a sulfate solution and determine the optimal nano-$CaCO_3$ content. The microscopic morphology and corrosion products of nano-$CaCO_3$ modified concrete's dry–wet transition areas were examined. A nonlinear surface model was used to quantify the relationship between the nano-$CaCO_3$ content and the relative dynamic elastic modulus for different areas of the concrete. Finally, the whole process of performance degradation of nano-$CaCO_3$ modified concrete was described in conjunction with the bivariate Wiener process, and reliability was analyzed. The findings of this study may contribute to the practical application of nano-$CaCO_3$ in concrete to improve sulfate attack resistance.

2. Experimental Details

2.1 Materials and Mix Proportions

In this study, P·O42.5 Portland cement, whose chemical composition is presented in Table 1, was used as the concrete binder. Class II fly ash was used as an additive. Local river sand with a fineness modulus of 2.9 was utilized as the fine aggregate, and broken pebbles with a 6 – 15 mm continuous gradation size were adopted as the coarse aggregate. Tap water was used as the mixing water.

Table 1. Chemical Composition of P·O 42.5 Portland Cement (% by mass)

Component	Loss	SiO_2	Al_2O_3	Fe_2O_3	CaO	MgO	SO_3	Na_2O
Content	1.92	24.08	8.54	4.01	58.29	1.73	2.85	0.5

Table 2. Performance Indices of Nano-$CaCO_3$

Appearance	Average particle size (nm)	Mass fraction (%)	Specific surface area (m^2/g)
White powder	≤60	≥99.0	30

Fig. 1. Appearance of Nano-$CaCO_3$

A polycarboxylate superplasticizer with a 25% water reduction rate was used as a chemical additive. Nano-$CaCO_3$ was purchased from the market for partial cement replacement, and its performance indices are presented in Table 2. A photograph of nano-$CaCO_3$ is shown in Fig. 1.

The mixture proportions for the tests were based on JGJ 55-2011, GB/T 50080-2016, and GB/T 50107-2010. Table 3 presents the concrete mixture proportions. Shaikh and Supit (2015) found that concrete containing 1% nano-$CaCO_3$ had the highest compressive strength, and Sun et al. (2020) study also came to the same conclusion. Wu et al. (2021) reported that, the compressive strength of ultrahigh-performance concrete increased as the nano-$CaCO_3$ content increased from 0 – 3.2%. As indicated by these results, there is an optimal value for the nano-$CaCO_3$ content. Thus, to determine the optimal amount of nano-$CaCO_3$ partial replacement for cement, nano-$CaCO_3$ contents in the range of 1 – 5% were used in this study.

2.2 Specimen Preparation and Curing Conditions

The large specific surface area of nano-$CaCO_3$ makes it prone to

Table 3. Mixture Proportions

Specimen	*w/b*	Cement (kg/m^3)	Fly ash (kg/m^3)	Nano-$CaCO_3$ (kg/m^3)	Broken pebbles (kg/m^3)	Sand (kg/m^3)	Water (kg/m^3)	Superplasticizer (kg/m^3)
H0	0.36	375	45	0	1,177	662	151	3.34
H1	0.36	370.8	45	4.2	1,177	662	151	3.34
H2	0.36	366.6	45	8.4	1,177	662	151	3.34
H3	0.36	358.2	45	12.6	1,177	662	151	3.34
H4	0.36	349.8	45	16.8	1,177	662	151	3.34
H5	0.36	337.2	45	21	1,177	662	151	3.34

agglomeration (Shaikh and Supit, 2014; Wu et al., 2021). In this study, emulating the method reported by Kawashima et al. (2014), nano-$CaCO_3$ was poured into a mixture composed of water and a water-reducing agent with a glass rod stirring for 2 min, and the mixture was then dispersed by an ultrasonic disperser for 15 min before being poured into a beaker. The cement, fly ash, and aggregate were weighed in turn, put into a concrete mixer, and mixed for 3 min. The mixture was slowly poured into the mixer and stirred for 3 min before it was shaken and loaded into the test molds. The specimens were removed after 24 h. The specimens were maintained at 95% relative humidity and 20 ± 3°C for 28 d before the partial-exposure test.

During the concrete preparation process, the larger specific surface area of nano-$CaCO_3$ causes free water and superplasticizer to adsorb on the surface of nano-$CaCO_3$, resulting in a decrease in the flowability of concrete. To ensure that the flowability of concrete meets requirements, slump flow tests were conducted according to the relevant provisions of GB/T 50080-2016. The tests found that the slump flow of concrete with different nano-$CaCO_3$ contents was all greater than 150 mm, indicating good workability and compliance with the requirements of GB 50164-2011.

2.3 Experimental Methods

The specimens were partially exposed to a 10% Na_2SO_4 solution. The part of the specimen exposed to air was denoted as the T area, the part in dry–wet transition was denoted as the M area, and was the part fully immersed in the solution was denoted as the D area. The test period was 360 d. Fig. 2 shows some specimens partially exposed. To ensure the accuracy of the test results, water was added to the test chamber every 30 d to maintain the water level of the solution.

Before data were collected, the surfaces of the specimens were cleaned. Every 60 d, a compression-testing machine was used to measure the compressive strength and flexural strength of three specimens with dimensions of 40 mm × 40 mm × 160 mm. Fig. 3(a) shows the test position. Every 60 d, an electronic balance was used to measure the mass of three specimens with dimensions of 100 mm × 100 mm × 400 mm. Every 60 d, an ultrasonic flaw detector was used to measure the ultrasonic velocities in the T area, M area, and D area for three specimens with dimensions of 100 mm × 100 mm × 400 mm. Fig. 3(b) shows the test position. In each case, three specimens were tested and the average value

Fig. 2. Specimen Partially Exposed to a Sulfate Solution

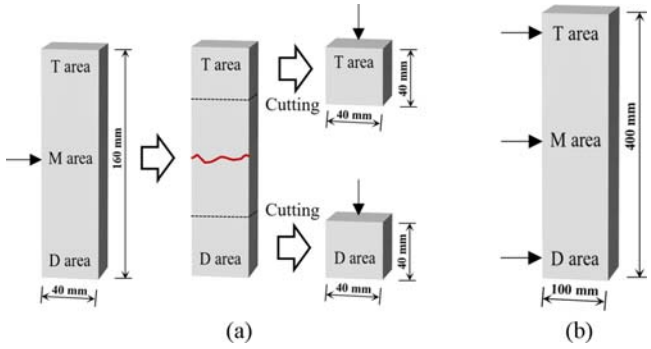

Fig. 3. Test Position of Specimen: (a) Test Position of Flexural Strength and Compressive Strength, (b) Test Position of Ultrasonic Velocities

was taken as the test result. Detailed average values of the specimens are available in Appendix.

2.4 Evaluation Parameters

The relative compressive strength evaluation parameter ω_1, relative flexural strength evaluation parameter ω_2, relative mass evaluation parameter ω_3, and relative dynamic elastic modulus evaluation parameter ω_4 were calculated using Eqs. (1) – (4), respectively:

$$\omega_1 = \frac{f_{\alpha r} - 0.75}{0.25} = \frac{f_{\alpha n} / f_{\alpha 0} - 0.75}{0.25}, \tag{1}$$

$$\omega_2 = \frac{f_{\beta r} - 0.75}{0.25} = \frac{f_{\beta n} / f_{\beta 0} - 0.75}{0.25}, \tag{2}$$

$$\omega_3 = \frac{w_r - 0.95}{0.05} = \frac{w_n / w_0 - 0.95}{0.05}, \tag{3}$$

$$\omega_4 = \frac{E_r - 0.60}{0.40} = \frac{V_n^2 / V_0^2 - 0.60}{0.40}, \tag{4}$$

where ω_1 is the relative compressive strength evaluation parameter, $f_{\alpha r}$ represents the relative compressive strength, $f_{\alpha n}$ represents the compressive strength of a specimen partially exposed for n days (MPa), and $f_{\alpha 0}$ represents the initial compressive strength of the specimen (MPa). ω_2 is the relative flexural strength evaluation parameter, $f_{\beta r}$ represents the relative flexural strength, $f_{\beta n}$ represents the flexural strength of a specimen partially exposed for n days (MPa), and $f_{\beta 0}$ represents the initial flexural strength of the specimen (MPa). ω_3 is the relative mass evaluation parameter, w_r represents the relative mass, w_n represents the mass of a specimen partially exposed for n days (kg), and w_0 represents the initial mass of the specimen (kg). ω_4 is the relative dynamic elastic modulus evaluation parameter, E_r represents the relative dynamic elastic modulus, V_n represents the ultrasonic velocity of a specimen partially exposed for n days (km/s), and V_0 represents the initial ultrasonic velocity of the specimen (km/s).

According to GB/T 50082-2009, when the relative compressive strength $f_{\alpha r}$, relative flexural strength $f_{\beta r}$, relative mass w_r, and relative dynamic elastic modulus E_r losses reach 0.25, 0.25, 0.05,

and 0.40, respectively, the specimen is considered to be damaged. Therefore, when ω_1, ω_2, ω_3, $\omega_4 > 1$, the specimen is considered to be in a reliable state; when $0 < \omega_1$, ω_2, ω_3, $\omega_4 < 1$, the specimen is considered to be in a damaged state; and when ω_1, ω_2, ω_3, $\omega_4 \leq 0$, the specimen is considered to be in a failure state.

2.5 Microstructure Analysis

The surfaces of the specimens were cleaned with a soft brush after the test. Samples of the broken specimens were collected from the M area (depth of 15 mm), and gold was sprayed after 48 h of natural air drying. SEM was used to examine the specimens. Additionally, the specimens were subjected to X-ray diffraction (XRD) analysis (scanning range of 10 – 90°) after the collection of the white material in the M area and the grinding of the broken sample of the M area (depth of 0 – 15 mm).

3. Results and Discussion

3.1 Results for Relative Compressive Strength Evaluation Parameter

The results for the relative compressive strength evaluation parameter of concrete with different nano-$CaCO_3$ contents partially exposed to a sulfate solution over time are presented in Fig. 4. As shown, the ω_1 value increased with the addition of 0 – 3% nano-$CaCO_3$ and decreased when the nano-$CaCO_3$ content was >3%.

As indicated by Fig. 4(a), the $\omega_{1\text{-T area}}$ values of the specimens increased from 0 to 180 d, with H1 and H5 exhibiting the largest and smallest increases, respectively. The $\omega_{1\text{-T area}}$ values of the specimens decreased from 180 to 360 d. At 360 d, the $\omega_{1\text{-T area}}$ values of the specimens decreased in the following order: 1 > H1 > H3 > H2 > H0 > H4 > H5 > 0. As shown in Fig. 4(b), the $\omega_{1\text{-D area}}$ values of the specimens increased from 0 to 180 d, with H1 and H2 exhibiting the largest and smallest increases, respectively. The $\omega_{1\text{-D area}}$ values of the specimens decreased from 180 to 360 d. At 360 d, the $\omega_{1\text{-D area}}$ values of the specimens decreased in the following order: 1 > H1 > H2 > H3 > H0 > H4 > H5 > 0.

At 360 d, H1 had a $\omega_{1\text{-T area}}$ value of 0.574 and a $\omega_{1\text{-D area}}$ value of 0.793. H5 had a $\omega_{1\text{-T area}}$ value of 0.106 and a $\omega_{1\text{-D area}}$ value of 0.228. The value of the relative compressive strength evaluation parameter varied more significantly in the T areas of the specimens than in the D areas. This indicates that during the test, the specimen with dimensions of 40 mm × 40 mm × 160 mm suffered from sulfate attack in the T areas to a higher extent than in the D areas, producing more corrosion products and more serious deterioration of durability. The specimens were in a reliable state from 0 to 180 d. They gradually entered the damaged state from 180 to 360 d. According to the relative compressive strength evaluation parameter results for the specimens, the smallest reduction in the relative compressive strength evaluation parameter occurred when the nano-$CaCO_3$ content was 1%.

3.2 Results for Relative Flexural Strength Evaluation Parameter

The results for the relative flexural strength evaluation parameter of

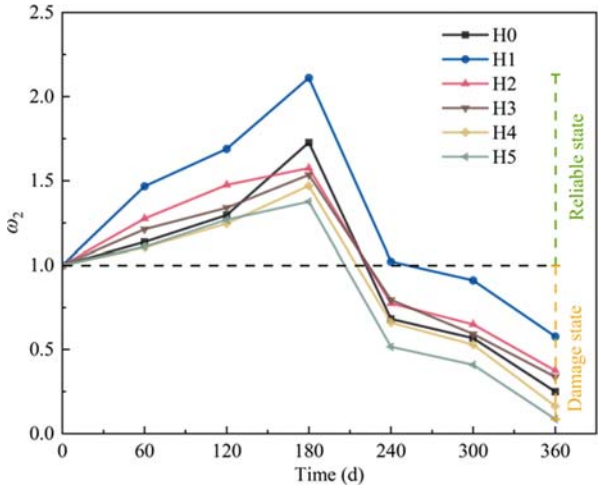

Fig. 5. Relative Flexural Strength Evaluation Parameter of Nano-$CaCO_3$ Modified Concrete

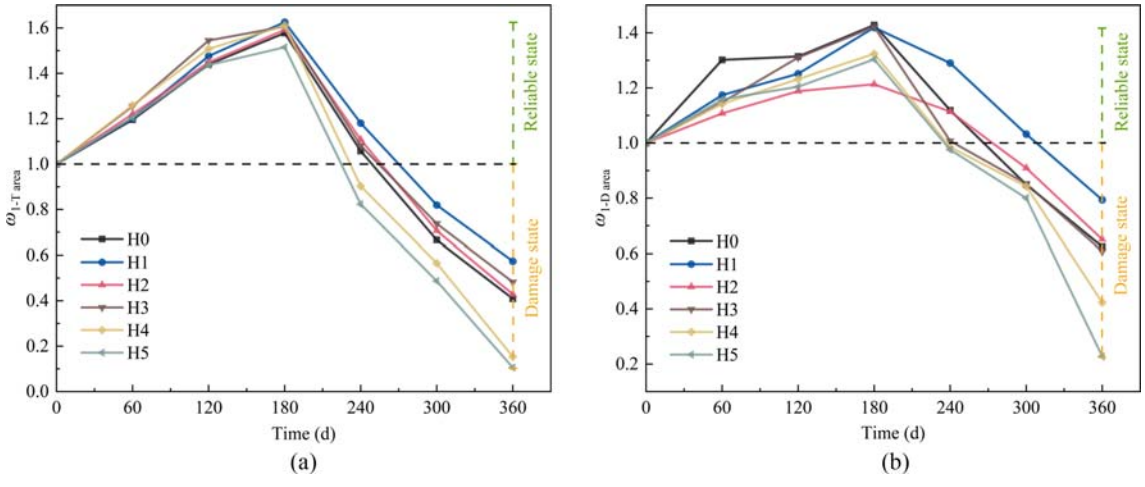

Fig. 4. Relative Compressive Strength Evaluation Parameter of Nano-$CaCO_3$ Modified Concrete: (a) ω_1 in the T Area of the Specimen, (b) ω_1 in the D Area of the Specimen

concrete with different nano-$CaCO_3$ contents partially exposed to a sulfate solution over time are presented in Fig. 5. As shown, the ω_2 values of the specimens increased with the addition of 0 – 3% nano-$CaCO_3$ and decreased when the nano-$CaCO_3$ content was >3%. The ω_2 values of the specimens increased from 0 to 180 d, with H1 and H5 exhibiting the largest and smallest increases, respectively. The ω_2 values of the specimens decreased from 180 to 360 d. At 360 d, the ω_2 values of the specimens decreased in the following order: 1 > H1 > H2 > H3 > H0 > H4 > H5 > 0. During the test, the specimens were in a reliable state from 0 to 180 d. They gradually entered the damaged state from 180 to 360 d. According to the relative flexural strength evaluation parameter results for the specimens, the smallest reduction in the relative flexural strength evaluation parameter occurred when the nano-$CaCO_3$ content was 1%.

3.3 Results for Relative Mass Evaluation Parameter

The results for the relative mass evaluation parameter of concrete with different nano-$CaCO_3$ contents partially exposed to a sulfate solution over time are presented in Fig. 6. As shown, the ω_3 values of the specimens increased with the addition of 0 – 2% nano-$CaCO_3$ and decreased when the nano-$CaCO_3$ content was >2%. The ω_3 values of the specimens increased from 0 to 180 d, with H1 and H5 exhibiting the largest and smallest increases, respectively. The ω_3 values of the specimens decreased from 180 to 360 d. At 360 d, the ω_3 values of the specimens decreased in

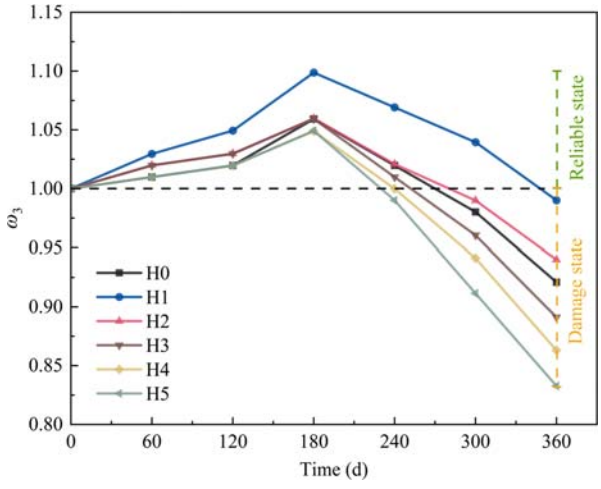

Fig. 6. Relative Mass Evaluation Parameter of Nano-$CaCO_3$ Modified Concrete

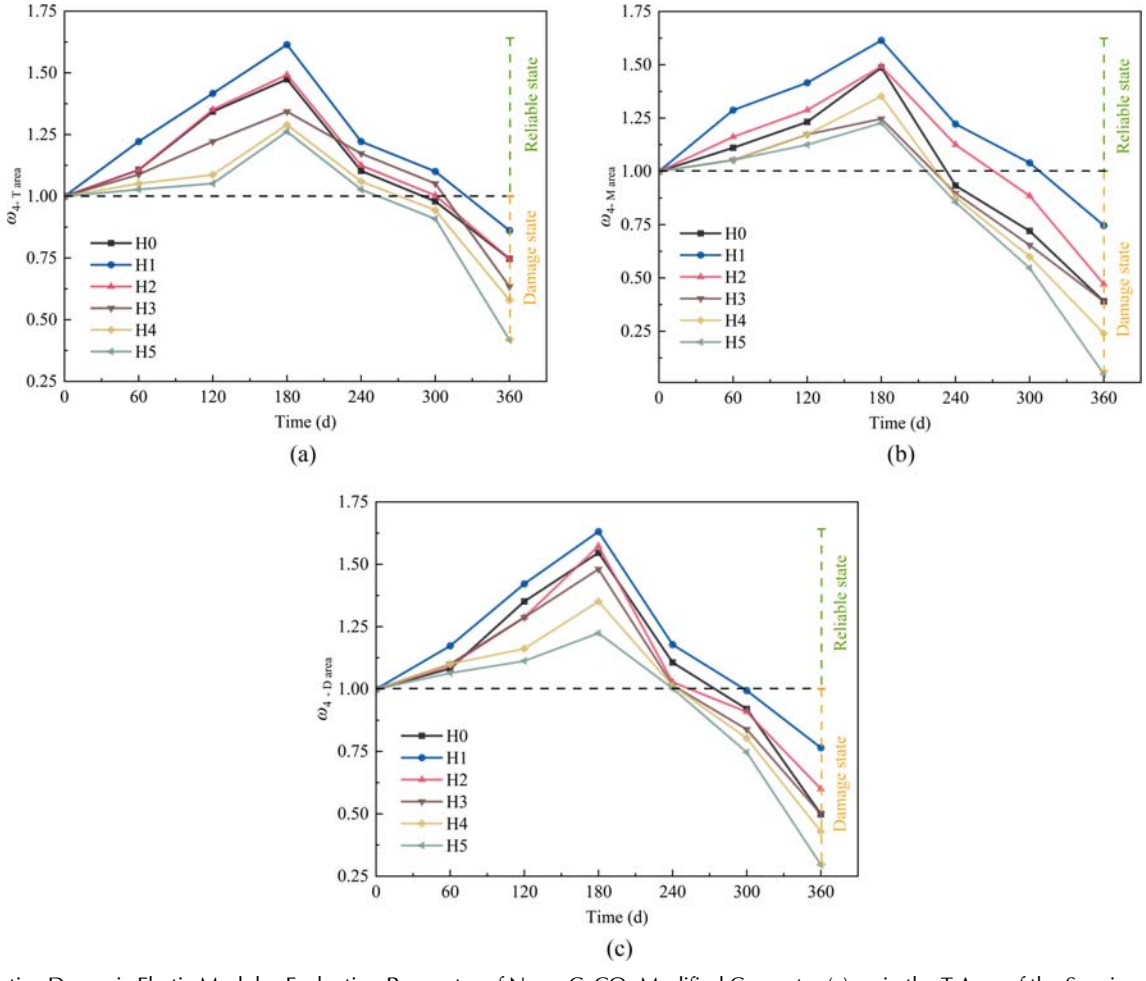

Fig. 7. Relative Dynamic Elastic Modulus Evaluation Parameter of Nano-$CaCO_3$ Modified Concrete: (a) ω_4 in the T Area of the Specimen, (b) ω_4 in the M Area of the Specimen, (c) ω_4 in the D Area of the Specimen

the following order: 1 > H1 > H2 > H0 > H3 > H4 > H5 > 0. During the test, the specimens were in a reliable state from 0 to 180 d. They gradually entered the damaged state from 180 to 360 d. According to the relative mass evaluation parameter results for the specimens, the smallest reduction in the relative mass evaluation parameter occurred when the nano-$CaCO_3$ content was 1%.

3.4 Results for Relative Dynamic Elastic Modulus Evaluation Parameter

The results for the relative dynamic elastic modulus evaluation parameter of concrete with different nano-$CaCO_3$ contents partially exposed to a sulfate solution over time are presented in Fig. 7. As shown, the ω_4 values of the specimens increased with the addition of 0 – 2% nano-$CaCO_3$ and decreased when the nano-$CaCO_3$ content was >2%. The $\omega_{4\text{-T area}}$ values of the specimens increased from 0 to 180 d, with H1 and H5 exhibiting the largest and smallest increases, respectively. The $\omega_{4\text{-T area}}$ values of the specimens decreased from 180 to 360 d. At 360 d, the $\omega_{4\text{-T area}}$ values of the specimens decreased in the following order: 1 > H1 > H2 > H0 > H3 > H4 > H5 > 0. The results for the $\omega_{4\text{-M area}}$ and $\omega_{4\text{-D area}}$ values of the specimens were similar to those for the $\omega_{4\text{-T area}}$ values.

At 360 d, H1 had a $\omega_{4\text{-T area}}$ value of 0.862, a $\omega_{4\text{-M area}}$ value of 0.746, and a $\omega_{4\text{-D area}}$ value of 0.765. H5 had a $\omega_{4\text{-T area}}$ value of 0.418, a $\omega_{4\text{-M area}}$ value of 0.050, and a $\omega_{4\text{-D area}}$ value of 0.296. The relative dynamic elastic modulus evaluation parameter varied more significantly in the M areas of the specimens than in the D and T areas. This indicates that during the test, the M areas of the specimens with dimensions of 100 mm × 100 mm × 400 mm suffered the highest degree of sulfate erosion. The M areas is the dry–wet transition, where the sulfate solution evaporates continuously, leading to the accumulation and increase of sulfate concentration, which causes a more serious sulfate attack. Compared with other areas, M areas have the most severe durability deterioration. A comparative analysis of the results for the ω_1, ω_2, and ω_4 values of the specimens indicated that the corrosion degrees of the different parts of nano-$CaCO_3$ modified concrete decreased in the following order: M area > D area > T area. During the test, the specimens were in a reliable state from 0 to 180 d. They gradually entered the damaged state from 180 to 360 d. At 360 d, the M area of H5 was almost in the failure state. According to the relative dynamic elastic modulus evaluation parameter results for the specimens, the smallest reduction in the relative dynamic elastic modulus evaluation parameter occurred when the nano-$CaCO_3$ content was 1%.

3.5 SEM Analysis

SEM images of concrete with different nano-$CaCO_3$ contents partially exposed to the sulfate solution for 360 d are presented in Fig. 8. The analysis area was the M area, and the magnification was 5000×. As shown, the specimens had different degrees of sulfate chemical attack, and the corrosion products generated were ettringite and gypsum. H3, H4, and H5 exhibited longer ettringite and gypsum parts than H0 (without the addition of nano-$CaCO_3$). Corrosion products cause microcracks and holes in concrete and intensify the sulfate chemical attack. This is consistent with the test results, which indicated that the nano-$CaCO_3$ content should not exceed 3%.

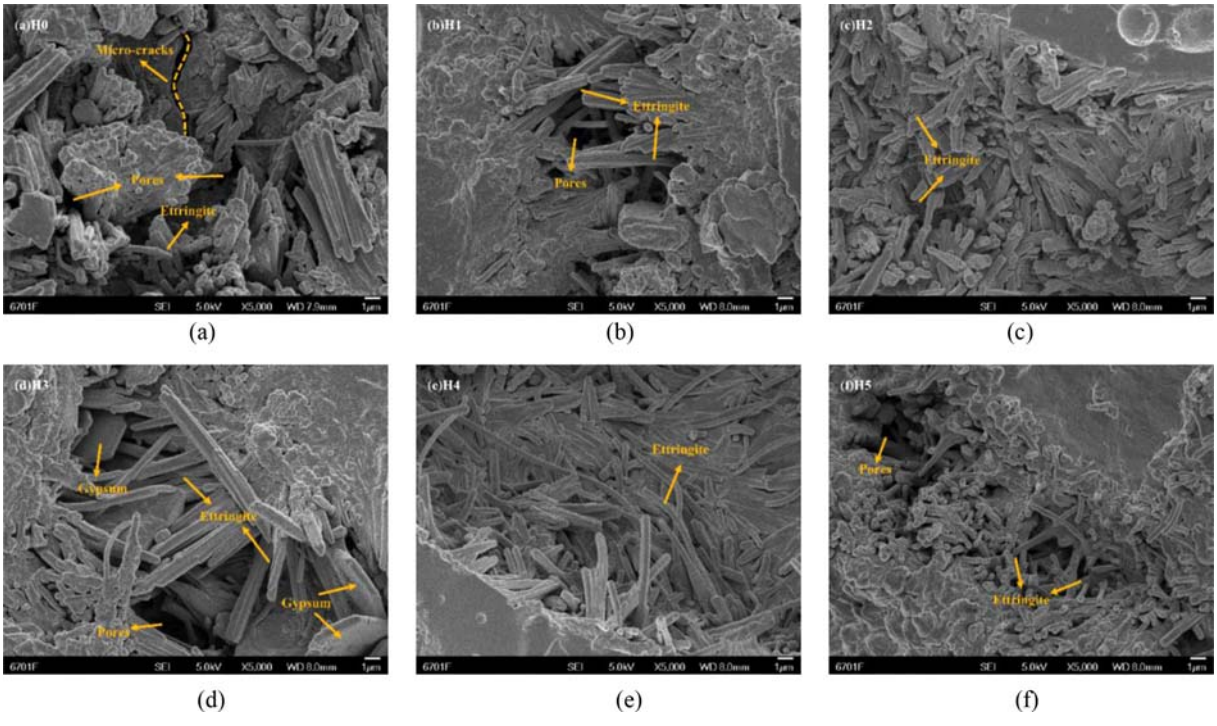

Fig. 8. SEM Images of Concrete with Different Nano-$CaCO_3$ Contents after Partial Exposure to the Sulfate Solution: (a) H0, (b) H1, (c) H2, (d) H3, (e) H4, (f) H5

3.6 XRD Micro-Analysis

XRD micro-analysis of the white material in the M area and on the surface of the M area of H1 partially exposed to the sulfate solution was performed, as shown in Figs. 9 and 10. The white material that precipitated from the concrete on the surface of the M area of H1 after the sulfate attack was $Na_2SO_4 \cdot 10H_2O$. This indicated that the sulfate physical attack occurred in the M area concrete. After the sulfate attack, the H1 corrosion products were mainly SiO_2, $CaCO_3$, $Ca(OH)_2$, ettringite, and $CaSO_4 \cdot 2H_2O$ (gypsum). SiO_2 is the main component of sand in concrete. $CaCO_3$ corresponds to the nano-$CaCO_3$ added to the concrete. $Ca(OH)_2$ is the hydration product of cement. Ettringite and $CaSO_4 \cdot 2H_2O$ (gypsum) are corrosion products of concrete. According to the test results and microscopic analysis, the deterioration in the M area of the nano-$CaCO_3$ modified concrete partially exposed to the sulfate solution was mainly due to the sulfate chemical attack and sulfate physical attack.

3.7 Sulfate Solution Transport Analysis

Wick action is the transport mechanism of water in partially exposed concrete (Liu et al., 2014). Water transport based on wick action involves capillary sorption and water vapor diffusion (Pel et al., 2004). According to the wick action, the sulfate solution transport in nano-$CaCO_3$ modified concrete can be classified into three types: the D area, M area, T area.

1. In the D area, the sulfate solution entered the concrete through capillary sorption, resulting in a concentration difference. This concentration difference accelerated the diffusion of the sulfate solution to the interior of the concrete. In this stage, the sulfate solution entered the D area via diffusion and capillary sorption (Bezerra and Azeredo, 2019; Ragoug et al., 2019).
2. The sulfate solution reached the M area through capillary sorption. After it reached the M area, the water gradually evaporated and formed a dry–wet interface on the concrete surface. The sulfate solution gradually accumulated, increasing the sulfate concentration at the dry–wet interface (Liu et al., 2014). As the concrete partial-exposure time increased, the sulfate chemical attack occurred in the M area concrete, and the sulfate physical attack occurred on the concrete surface and precipitated the white material $Na_2SO_4 \cdot 10H_2O$, as shown in the M area in Fig. 11(a). According to the results for the relative flexural strength evaluation parameter and the M area relative dynamic elastic modulus evaluation parameter, the M area concrete had the highest degree of corrosion.
3. The sulfate solution reached the T area through capillary sorption via the M area. Owing to the height of the T area, the capillary sorption rate decreased (Ma, 2009). According to the results for the T area relative compressive strength evaluation parameter and T area relative dynamic elastic modulus evaluation parameter, the amount of sulfate solution in the T area was smaller than those in the other areas, and the corrosion degree was the lowest. At 180 d, the white material $Na_2SO_4 \cdot 10H_2O$ did not appear on the T area surface of the specimen with dimensions of 100 mm × 100 mm × 400 mm, as shown in Fig. 11(a). However, it was observed on the T area surface of the specimen with dimensions of 40 mm × 40 mm × 160 mm, as shown in Fig. 11(b). When the partial-exposure time was sufficient for the surface concrete at the T area dry–wet interface to undergo the sulfate chemical attack (Liu et al., 2012), the

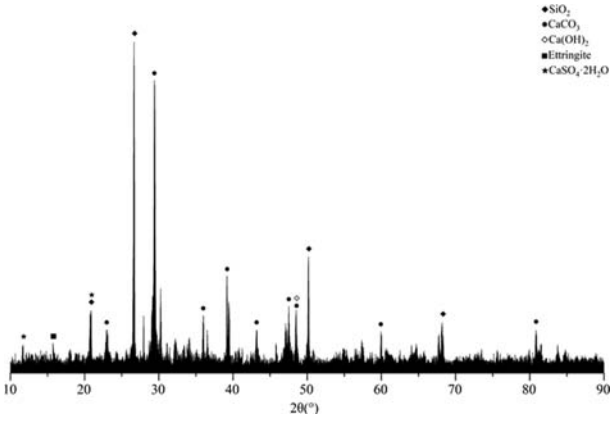

Fig. 9. XRD Micro-Analysis Results for H1 Specimens Partially Exposed to the Sulfate Solution

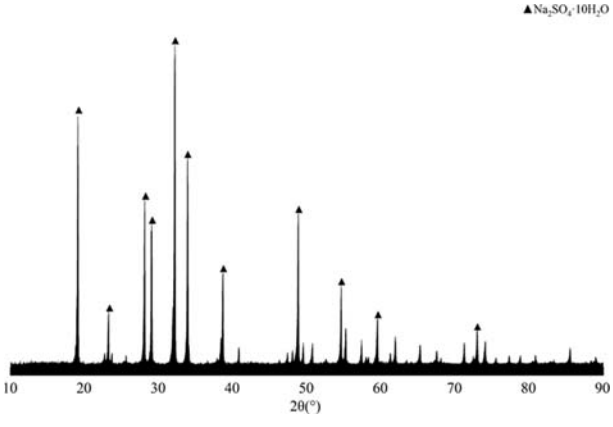

Fig. 10. XRD Micro-Analysis Results for the White Material on the Surface of the H1 Specimen Partially Exposed to the Sulfate Solution

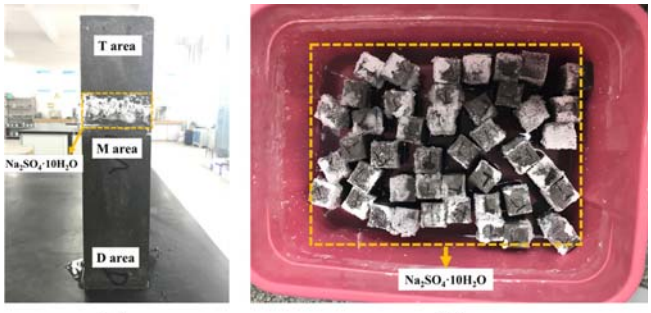

Fig. 11. Appearance of Nano-$CaCO_3$ Modified Concrete Partially Exposed to the Sulfate Solution at 180 d: (a) Dimensions of 100 mm × 100 mm × 400 mm Specimen Appearance, (b) Dimensions of 40 mm × 40 mm × 160 mm Specimen Appearance

surface concrete can gradually precipitate the white material $Na_2SO_4 \cdot 10H_2O$.

The sulfate solution gradually entered the concrete interior as the partial-exposure time increased. A sulfate chemical attack of the concrete in the D area, M area, and T area occurred, generating the corrosion products ettringite and gypsum. This resulted in the volume expansion of the original hydration products (Tian and Cohen, 2000). From 0 to 180 d, the corrosion products filled the internal defects of the concrete, enhanced its internal compactness, reduced its porosity, and enhanced its durability. The evaluation parameters for each specimen exhibited an increasing trend, and the specimens were in a reliable state. From 180 to 360 d, owing to the increase in the number of corrosion products within the concrete, the internal crystallization pressure in the concrete

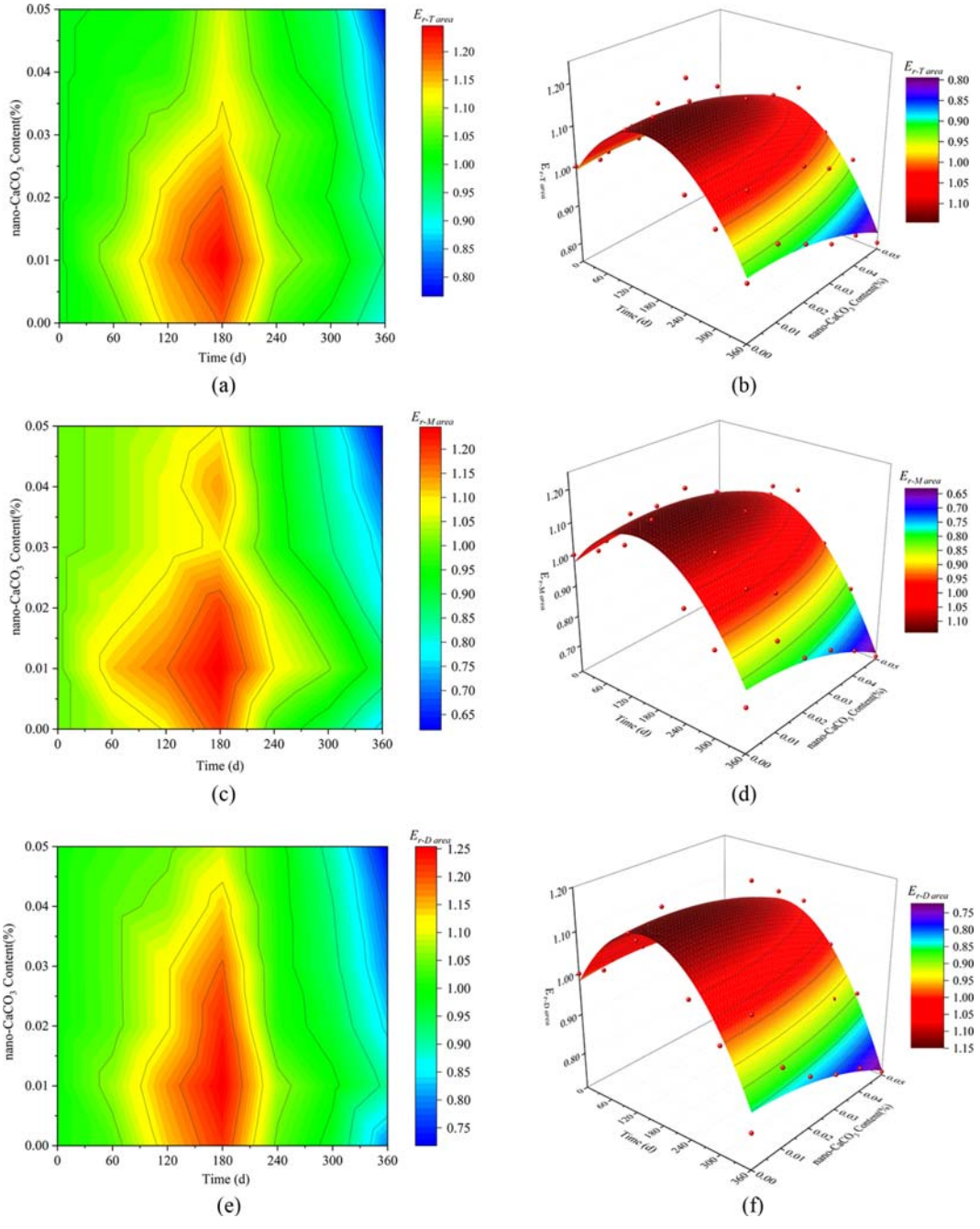

Fig. 12. Statistical Analysis of the Relative Dynamic Elastic Modulus for Different Areas of the Concrete: (a) Contour Map of the Partial Exposure Time and T Area Concrete Relative Dynamic Elastic Modulus, (b) Curved Surface Model Fitting Diagram of the Partial Exposure Time and T Area Concrete Relative Dynamic Elastic Modulus, (c) Contour Map of the Partial Exposure Time and M Area Concrete Relative Dynamic Elastic Modulus, (d) Curved Surface Model Fitting Diagram of the Partial Exposure Time and M Area Concrete Relative Dynamic Elastic Modulus, (e) Contour Map of the Partial Exposure Time and D Area Concrete Relative Dynamic Elastic Modulus, (f) Curved Surface Model Fitting Diagram of the Partial Exposure Time and D Area Concrete Relative Dynamic Elastic Modulus

increased, causing microcracks (Bellmann et al., 2006). The M area surface concrete was gradually subjected to the sulfate physical attack, intensifying the corrosion of the concrete, and concrete deterioration occurred until destruction. The evaluation parameters for each specimen exhibited a decreasing trend, and the specimens were in a damaged state.

4. Statistical Analysis of Test Results

To determine the optimal nano-$CaCO_3$ content more precisely, the characteristics of the partial-exposure test were combined. The nano-$CaCO_3$ content (NC) and partial-exposure time (T) were used as independent variables, and the relative dynamic elastic modulus (E_r) of the concrete in different areas partially exposed to the sulfate solution was selected as the dependent variable. The relationship between the nano-$CaCO_3$ content (NC) and the relative dynamic elastic modulus (E_r) of concrete in different areas was quantified via nonlinear surface model fitting.

Figure 12 presents the contour plot and nonlinear surface model fit diagram showing the effects of the nano-$CaCO_3$ content and partial-exposure time on the relative dynamic elastic modulus of different areas of the concrete. As the partial-exposure time increased, an appropriate nano-$CaCO_3$ content increased the relative dynamic elastic modulus of the concrete. Among the areas examined, the deterioration of the M area concrete relative dynamic elastic modulus at the dry–wet interface was the most severe during partial exposure to the sulfate solution. The relative dynamic elastic modulus of the concrete was the highest in the case of 1% nano-$CaCO_3$.

According to the fitting results, the regression equations for the nano-$CaCO_3$ content, partial-exposure time, and relative dynamic elastic modulus of different areas of the concrete were established (Eqs. (5) – (7)).

$$E_{r-T\ area} = 0.990 + 0.002 \times T + 1.417 \times NC - 5.849 \times 10^{-6} \times (T)^2 - 46.496 \times (NC)^2 - 0.004 \times T \times NC \quad (5)$$

$$E_{r-M\ area} = 0.976 + 0.002 \times T + 2.810 \times NC - 7.097 \times 10^{-6} \times (T)^2 - 64.552 \times (NC)^2 - 0.009 \times T \times NC \quad (6)$$

$$E_{r-D\ area} = 0.983 + 0.002 \times T + 1.511 \times NC - 6.987 \times 10^{-6} \times (T)^2 - 41.970 \times (NC)^2 - 0.005 \times T \times NC \quad (7)$$

Here, $E_{r\text{-}T\ area}$ represents the T area concrete relative dynamic elastic modulus, $E_{r\text{-}M\ area}$ represents the M area concrete relative dynamic elastic modulus, $E_{r\text{-}D\ area}$ represents the D area concrete relative dynamic elastic modulus, T represents the duration for which the concrete was partially exposed to the sulfate solution (d), and NC represents the nano-$CaCO_3$ content of the concrete.

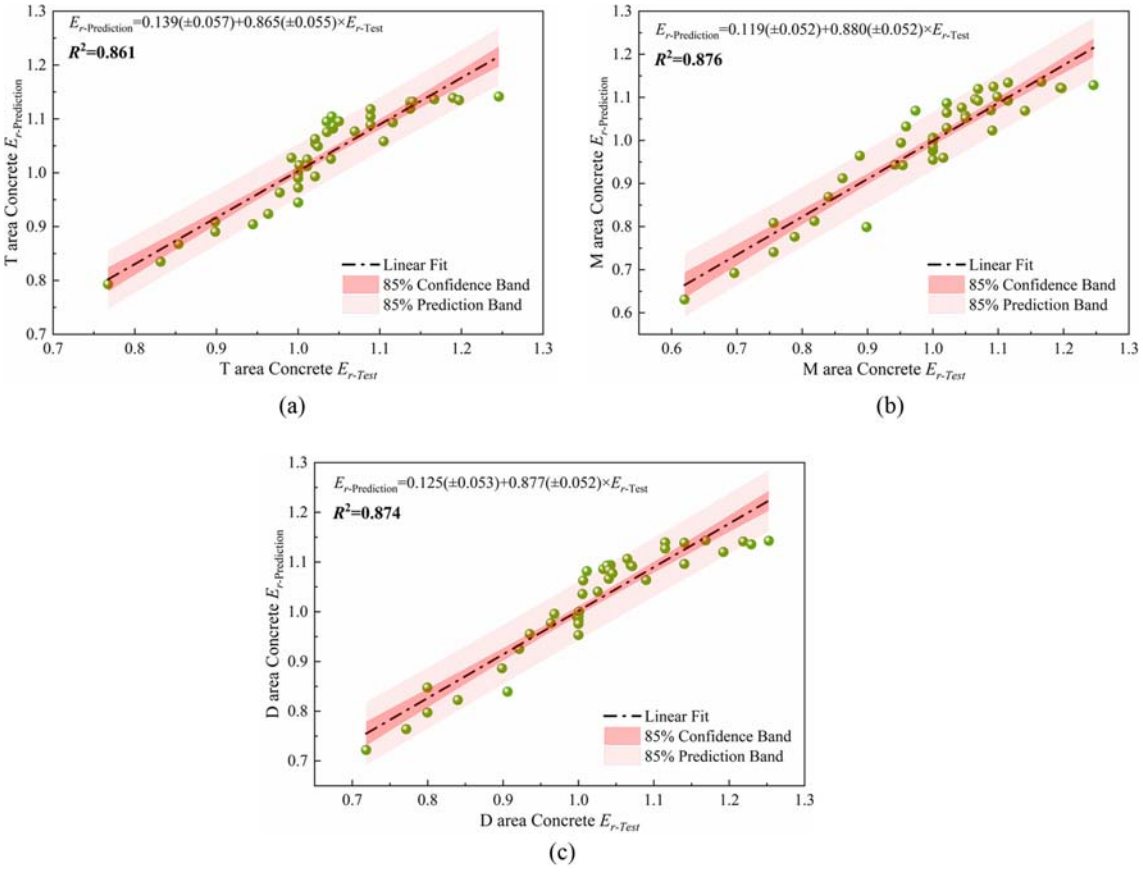

Fig. 13. Correlation Analysis of the Relative Dynamic Elastic Modulus for Different Areas of Concrete: (a) T Area Concrete, (b) M Area Concrete, (c) D Area Concrete

As shown in Fig. 13, the predicted values of the relative dynamic elastic modulus of the concrete in different areas were fitted to the test results to evaluate the accuracy of the regression equation. The fitting accuracy was high. The regression model provides guidance for the use of nano-$CaCO_3$ in concrete and provides a reference and basis for predicting the durability of concrete partially exposed to a sulfate solution. However, this model can only be used for predicting the relative dynamic elastic modulus for different areas of concrete that have been partially exposed to a 10% sulfate solution with a nano-$CaCO_3$ content in the range of 1 – 5%. For extending the model, the next step is to collect more experimental data.

5. Establishment of Bivariate Wiener process

5.1 Bivariate Wiener Process Theory

The degradation of concrete modified with nano-$CaCO_3$ in sulfate environments is the result of physical-chemical actions that can be effectively modeled using the Wiener process, provided that appropriate conditions are met. The degradation data of this type of concrete exhibit randomness and may be independent or correlated. As demonstrated in Section 2, the dry-wet transition areas (M area) of the concrete are the most severely affected. To address this, a bivariate Wiener process was employed to model the degradation data of nano-$CaCO_3$ modified concrete in the M area, including the relative dynamic elastic modulus ($E_{r\text{-}M\ area}$) and relative flexural strength ($f_{\beta r}$). The detailed modeling process is as follows (Peng, 2010; Sacerdote et al., 2016):

Let $X(t) = (x_1(t), x_2(t))'$ represent the degradation data of nano-$CaCO_3$ modified concrete, satisfying the following properties:

1. The degradation increments $\Delta X(t) = X(t) - X(t + \Delta t)$ follow a bivariate normal distribution $N(\boldsymbol{\mu}\Delta t, \boldsymbol{\Sigma}\Delta t)$.
2. The degradation increments $\Delta X(t)$ for any two disjoint periods are independent and identically distributed.
3. $X(t)$ is continuous at $t = 0$.

Here, x_1 represents the M area concrete relative dynamic elastic modulus ($E_{r\text{-}M\ area}$); x_2 represents relative flexural strength ($f_{\beta r}$); $\boldsymbol{\mu} = (\mu_1, \mu_2)$; $\boldsymbol{\Sigma} = \begin{bmatrix} \sigma_1^2 & C_{12} \\ C_{21} & \sigma_2^2 \end{bmatrix}$; μ_1 and μ_2 are the respective mean values of ΔX_1 and ΔX_2; σ_1 and σ_2 are the respective variances of ΔX_1 and ΔX_2; C_{12} and C_{21} are the covariances between degradation data x_1 and x_2.

The degradation increments of $E_{r\text{-}M\ area}$ and $f_{\beta r}$ in concrete, which was modified with nano-$CaCO_3$, were assessed using a Q-Q plot, as shown in Fig. 14. The Q-Q plot demonstrated that the degradation increments complied with a one-dimensional normal distribution. Therefore, it was concluded that the degradation increments of nano-$CaCO_3$ modified concrete satisfy a bivariate normal distribution. Consequently, the degradation process of concrete modified with nano-$CaCO_3$ can be accurately described using a bivariate Wiener process.

Failure is determined when the degradation data (x) of nano-$CaCO_3$ modified concrete reaches the failure threshold (l) for the

Table 4. Degradation Increments of $E_{r\text{-}M\ area}$

Specimen	0 d	60 d	120 d	180 d	240 d	300 d	360 d
H0	0	0.044	0.049	0.102	-0.168	0.085	0.132
H1	0	0.115	0.051	0.080	-0.157	-0.073	0.086
H2	0	0.065	0.050	0.082	-0.147	-0.004	0.166
H3	0	0.021	0.048	0.029	-0.058	0.097	0.106
H4	0	0.021	0.048	0.072	-0.092	0.111	0.144
H5	0	0.021	0.029	0.041	-0.033	0.123	0.199

Table 5. Degradation Increments of $f_{\beta r}$

Specimen	0 d	60 d	120 d	180 d	240 d	300 d	360 d
H0	0	0.034	0.040	0.108	-0.102	0.028	0.080
H1	0	0.117	0.056	0.106	-0.032	0.017	0.083
H2	0	0.069	0.050	0.025	-0.088	0.031	0.069
H3	0	0.053	0.027	0.054	-0.083	0.051	0.064
H4	0	0.026	0.034	0.058	-0.033	0.033	0.092
H5	0	0.027	0.043	0.024	0.027	0.027	0.081

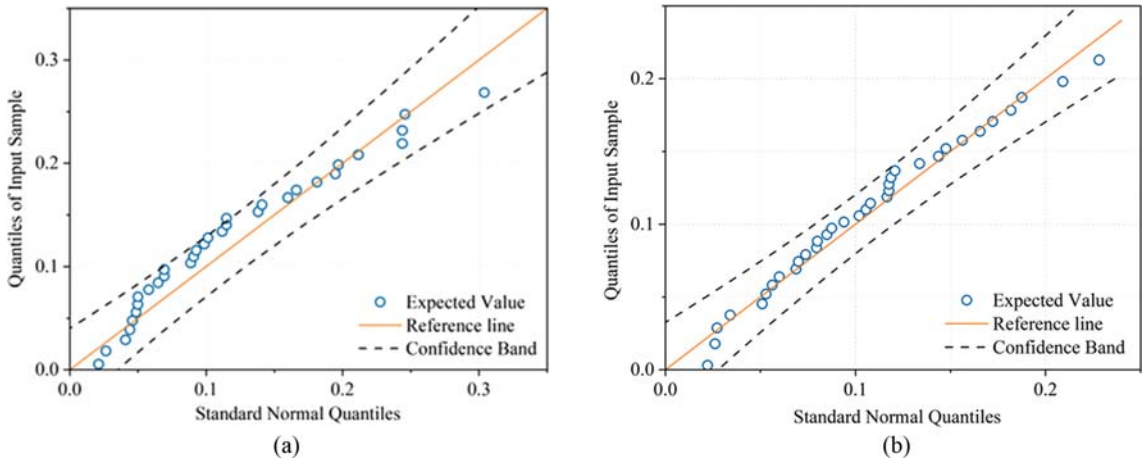

Fig. 14. Q-Q Plot of Degradation Increments: (a) $E_{r\text{-}M\ area}$, (b) $f_{\beta r}$

first time. The failure thresholds are defined as $l_1 = 0.4$ and $l_2 = 0.25$, as described in Section 2.4. The failure time (T) is defined as the time at which degradation data (x_1 or x_2) first reaches its respective failure threshold (l_1 or l_2).

$$T = \inf\{t : X_1(t) > l_1 \text{ or } X_2(t) > l_2\} \tag{8}$$

The correlation between degradation data is determined by the covariance, $C_{ij} = \text{cov}(x_i, x_j)$. Non-zero values of C_{ij} indicate a positive correlation between the degradation data, while values close to or equal to zero suggest a weak correlation. Previous studies (Hu et al., 2007) have suggested that a correlation between degradation data is insignificant when $C_{ij} \leq 0.3$. As such, given that $C_{12} = C_{21} = 0.0148 \leq 0.3$ for x_1 and x_2, it can be concluded that the $E_{r\text{-}M\,area}$ and $f_{\beta r}$ degradation processes in nano-$CaCO_3$ modified concrete are independent of each other. Thus, it is sufficient to consider a tandem model comprising of reliability models for individual degradation data while modeling their reliability (Peng, 2010).

The degradation process of nano-$CaCO_3$ modified concrete performance can be modeled as a one-dimensional Wiener process when considering only individual degradation data. The reliability function $R(t)$ for the degradation process is given by Eq. (9) (Wang et al., 2022).

$$R(t) = \Phi\left(\frac{l-\mu t}{\sigma\sqrt{t}}\right) - \exp\left(\frac{2\mu l}{\sigma^2}\right)\Phi\left(\frac{-l-\mu t}{\sigma\sqrt{t}}\right) \tag{9}$$

When considering the degradation data x_1 and x_2 together, the reliability function $R(t)$ of the nano-$CaCO_3$ modified concrete performance degradation process can be modeled using Eq. (10) (Peng, 2010).

$$R(t) = R_1(t)R_2(t) = \left[\Phi\left(\frac{l_1-\mu_1 t}{\sigma_1\sqrt{t}}\right) - \exp\left(\frac{2\mu_1 l_1}{\sigma_1^2}\right)\Phi\left(\frac{-l_1-\mu_1 t}{\sigma_1\sqrt{t}}\right)\right] \left[\Phi\left(\frac{l_2-\mu_2 t}{\sigma_2\sqrt{t}}\right) - \exp\left(\frac{2\mu_2 l_2}{\sigma_2^2}\right)\Phi\left(\frac{-l_2-\mu_2 t}{\sigma_2\sqrt{t}}\right)\right] \tag{10}$$

Here, $R_1(t)$ and $R_2(t)$ respective represent the reliability functions when considering only x_1 and x_2.

The lifetime distribution function for nano-$CaCO_3$ modified concrete is expressed by Eq. (11).

$$F(t) = 1 - R(t) \tag{11}$$

The probability density function of nano-$CaCO_3$ modified concrete is described by Eq. (12).

$$f(t) = \frac{\mathrm{d}F(t)}{t} \tag{12}$$

5.2 Parameter Estimation

A partially exposed sulfate attack test was conducted on n specimens of nano-$CaCO_3$ modified concrete. For specimen i, the amount of performance degradation data $x_1(t)$ was measured at moment $t_{i1}^{(1)}, t_{i2}^{(1)}, \cdots, t_{im_{1i}}^{(1)}$, and its corresponding value, $x_{i1}^{(1)}, x_{i2}^{(1)}, \cdots, x_{im_{1i}}^{(1)}$, was recorded. Similarly, for specimen j, the amount of performance degradation data $x_2(t)$ was measured at moment $t_{i1}^{(2)}, t_{i2}^{(2)}, \cdots, t_{im_{2i}}^{(2)}$, and its corresponding value, $x_{i1}^{(2)}, x_{i2}^{(2)}, \cdots, x_{im_{2i}}^{(2)}$, was recorded.

Given that the $E_{r\text{-}M\,area}$ and $f_{\beta r}$ degradation processes of nano-$CaCO_3$ modified concrete are independent of each other, it is possible to model individual degradation data using a one-dimensional Wiener process. Let $\Delta X_{ij}^{(k)} = x_{ij}^{(k)} - x_{i(j-1)}^{(k)}$ represent the degradation increments of specimen i between moments $\Delta t_{ij}^{(k)} = t_{ij}^{(k)} - t_{i(j-1)}^{(k)}$ (where $j = 1, 2, \cdots, m_{ki}, k = 1, 2$).

The probability density likelihood function for a given moment can be obtained from Eq. (12) as follows:

$$L(\mu_k, \sigma_k^2) = \prod_{i=1}^{n}\prod_{j=1}^{m_{ki}} \frac{1}{\sqrt{2\sigma_k^2 \pi \Delta t_{ij}^{(k)}}} \exp\left[-\frac{(\Delta X_{ij}^{(k)} - \mu_k \Delta t_{ij}^{(k)})^2}{2\sigma_k^2 \Delta t_{ij}^{(k)}}\right] \tag{13}$$

Equation (14) is obtained by solving the logarithmic form of Eq. (13).

$$\hat{\mu}_k = \frac{\sum_{i=1}^{n} x_{im_{ki}}^{(k)}}{\sum_{i=1}^{n} t_{im_{ki}}^{(k)}}, \hat{\sigma}_k^2 = \frac{1}{\sum_{i=1}^{n} m_{ki}}\left[\sum_{i=1}^{n}\sum_{j=1}^{m_{ki}} \frac{(\Delta X_{ij}^{(k)})^2}{\Delta t_{ij}^{(k)}} - \frac{\left(\sum_{i=1}^{n} x_{im_{ki}}^{(k)}\right)^2}{\sum_{i=1}^{n} t_{im_{ki}}^{(k)}}\right] \tag{14}$$

The drift parameter μ and diffusion parameter σ for H0 – H5 were calculated by solving Eq. (14), and their corresponding values are presented in Table 6.

5.3 Reliability Analysis

The obtained drift parameter μ and diffusion parameter σ from Table 6 were used to compute the reliability of nano-$CaCO_3$ modified concrete using Eq. (10), and the results are presented in Fig. 15. It is important to note that reliability refers to the ability of concrete to function normally within the designed service life. During the partial exposure to sulfate attack test, the relative dynamic elastic modulus $E_{r\text{-}M\,area}$ and the relative flexural strength $f_{\beta r}$ of the M area concrete specimens initially increased, then decreased as the SO_4^{2-} in the solution continuously attacked the concrete. Consequently, the reliability of the concrete gradually declined, indicating an increase in its corrosion level. When reliability is zero, it indicates that the concrete can no longer meet the normal usage requirements, reaching a failure state. At this point, the

Table 6. Parameter Estimates

Degradation data		H0	H1	H2	H3	H4	H5
$E_{r\text{-}M\,area}$	μ	6.77E-04	2.82E-04	5.88E-04	6.77E-04	8.44E-04	1.06E-03
	σ	1.27E-02	1.27E-02	1.24E-02	7.01E-03	9.73E-03	9.82E-03
$f_{\beta r}$	μ	5.21E-04	2.93E-04	4.34E-04	4.60E-04	5.81E-04	6.34E-04
	σ	8.52E-03	1.73E-02	6.90E-03	6.53E-03	4.82E-03	2.58E-03

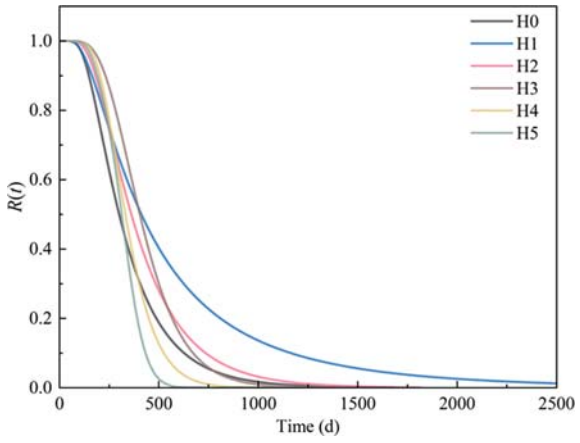

Fig. 15. Reliability Function Curve for Nano-$CaCO_3$ Modified Concrete

service life of the specimens, ordered from the longest to the shortest, was H1 > H2 > H0 > H3 > H4 > H5, with H1 achieving the longest service life of 2487 days and H5 attaining the shortest service life of 540 days. These findings imply that a 1% content of nano-$CaCO_3$ achieved the longest concrete service life. When nano-$CaCO_3$ is excessive, it is difficult to disperse uniformly, leading to increased viscosity and agglomeration issues, introducing obvious cracks and pore between the matrix and aggregates, resulting in higher porosity in concrete (Wu et al., 2016; Wu et al., 2018). This leads to a decrease in concrete durability performance, reducing the service life of concrete. The criteria for determining concrete reliability using the bivariate Wiener process can be improved and used to guide the repair and reinforcement of actual concrete structures to extend their service life.

6. Conclusions

In this study, the durability of different areas of concrete with different nano-$CaCO_3$ contents partially exposed to a sulfate solution was investigated. The following conclusions are drawn.

1. According to the results for the relative compressive strength, relative flexural strength, relative mass, and relative dynamic elastic modulus evaluation parameters, there is an optimal nano-$CaCO_3$ content. In this study, the concrete had the highest durability when the nano-$CaCO_3$ content was 1%.
2. Test results indicated that the corrosion degrees of different areas of the nano-$CaCO_3$ modified concrete partially exposed to the sulfate solution decreased in the following order: M area > D area > T area. SEM and XRD analysis results indicated that the sulfate chemical attack and sulfate physical attack occurred in the dry–wet transition areas (M area) of concrete, generating the corrosion products ettringite and gypsum, precipitating $Na_2SO_4 \cdot 10H_2O$.
3. Regression equations for the nano-$CaCO_3$ content, partial-exposure time, and relative dynamic elastic modulus in different areas of the concrete were established via nonlinear surface model fitting. The fitting results indicated that the established regression equations have high accuracy. The relative dynamic elastic modulus for different areas of nano-$CaCO_3$ modified concrete was predicted using the regression equations. Comparisons revealed a strong correlation between the predicted values and test results.
4. The bivariate Wiener process effectively characterizes the entire performance deterioration process of nano-$CaCO_3$ modified concrete partially exposed to sulfate solution. Moreover, the service life of the specimen, ranked in decreasing order from longest to shortest, was H1 > H2 > H0 > H3 > H4 > H5, with H1 having the longest service life of 2487 days and H5 having the shortest service life of 540 days when the reliability is 0.

Acknowledgments

The authors would like to express their gratitude to the National Natural Science Foundation of China (Nos. 51468039, 51868044).

ORCID

Bo Yang http://orcid.org/0000-0003-2595-3740
Hongxia Qiao http://orcid.org/0000-0002-0289-1949

References

Bassuoni MT, Rahman MM (2016) Response of concrete to accelerated physical salt attack exposure. *Cement and Concrete Research* 79:395-408, DOI: 10.1016/j.cemconres.2015.02.006

Bellmann F, Möser B, Stark J (2006) Influence of sulfate solution concentration on the formation of gypsum in sulfate resistance test specimen. *Cement and Concrete Research* 36(2):358-363, DOI: 10.1016/j.cemconres.2005.04.006

Bezerra WVDC, Azeredo GA (2019) External sulfate attack on compressed stabilized earth blocks. *Construction and Building Materials* 200:255-264, DOI: 10.1016/j.conbuildmat.2018.12.115

Camiletti J, Soliman AM, Nehdi ML (2013) Effects of nano- and micro-limestone addition on early-age properties of ultra-high-performance concrete. *Materials and Structures* 46(6):881-898, DOI: 10.1617/s11527-012-9940-0

Chang C, An L, Zheng W, Wen J, Dong J, Yan F, Xiao X (2021) Research and engineering application of salt erosion resistance of magnesium oxychloride cement concrete. *Materials* 14(24):7880, DOI: 10.3390/ma14247880

Chen F, Gao J, Qi B, Shen D (2017) Deterioration mechanism of plain and blended cement mortars partially exposed to sulfate attack. *Construction and Building Materials* 154:849-856, DOI: 10.1016/j.conbuildmat.2017.08.017

Ding Y, Liu J-P, Bai Y-L (2020) Linkage of multi-scale performances of nano-$CaCO_3$ modified ultra-high performance engineered cementitious composites (UHP-ECC). *Construction and Building Materials* 234:117418, DOI: 10.1016/j.conbuildmat.2019.117418

Hu JT, Hu CH, Chen L, Zhang JB (2007) Study on reliability evaluation approach based on multivariate degradation measures. *Control Engineering of China* S3:77-79+92 (in Chinese)

Kawashima S, Hou P, Corr DJ, Shah SP (2013) Modification of cement-based materials with nanoparticles. *Cement and Concrete Composites*

36:8-15, DOI: 10.1016/j.cemconcomp.2012.06.012
Kawashima S, Seo J-WT, Corr D, Hersam MC, Shah SP (2014) Dispersion of $CaCO_3$ nanoparticles by sonication and surfactant treatment for application in fly ash–cement systems. *Materials and Structures* 47(6):1011-1023, DOI: 10.1617/s11527-013-0110-9
Li G, Zhuang Z, Lv Y, Wang K, Hui D (2020) Enhancing carbonation and chloride resistance of autoclaved concrete by incorporating Nano-$CaCO_3$. *Nanotechnology Reviews* 9(1):998-1008, DOI: 10.1515/ntrev-2020-0078
Liang JZ (2007) Evaluation of dispersion of nano-$CaCO_3$ particles in polypropylene matrix based on fractal method. *Composites Part A: Applied Science and Manufacturing* 38(6):1502-1506, DOI: 10.1016/j.compositesa.2007.01.011
Liu Z, Deng D, De Schutter G (2014) Does concrete suffer sulfate salt weathering? *Construction and Building Materials* 66:692-701, DOI: 10.1016/j.conbuildmat.2014.06.011
Liu Z, Deng D, Schutter GD, Yu Z (2012) Chemical sulfate attack performance of partially exposed cement and cement+fly ash paste. *Construction and Building Materials* 28(1):230-237, DOI: 10.1016/j.conbuildmat.2011.08.071
Ma K (2009) Mechanism and evaluation method of salt crystallization attack on concrete. PhD Thesis, Central South University, Changsha, China (in Chinese)
Mehairi AG, Husein MM (2020) Enhancement of cement properties by means of in situ grown nanoparticles. *Construction and Building Materials* 261:120496, DOI: 10.1016/j.conbuildmat.2020.120496
Pavan Kumar D, Amit S, Sri Rama Chand M (2021) Influence of various nano-size materials on fresh and hardened state of fast setting high early strength concrete [FSHESC]: A state-of-the-art review. *Construction and Building Materials* 277:122299, DOI: 10.1016/j.conbuildmat.2021.122299
Pel L, Huinink H, Kopinga K, van Hees RPJ, Adan OCG (2004) Efflorescence pathway diagram: Understanding salt weathering. *Construction and Building Materials* 18(5):309-313, DOI: 10.1016/j.conbuildmat.2004.02.003
Peng BH (2010) Research on reliability modeling methods based on wiener process. PhD Thesis, Graduate School of National University, Changsha, China (in Chinese)
Qinghai Institute of Salt Lakes (QISL), Chinese Academy of Sciences (CAS) (2015) Chinese academy of sciences salt lake research for 60 Years. Science China Press Ltd, Beijing, China, 27-33
Ragoug R, Metalssi OO, Barberon F, Torrenti J-M, Roussel N, Divet L, d'Espinose de Lacaillerie J-B (2019) Durability of cement pastes exposed to external sulfate attack and leaching: Physical and chemical aspects. *Cement and Concrete Research* 116:134-145, DOI: 10.1016/j.cemconres.2018.11.006
Rong Z, Jiang G, Sun W (2015) Effects of nano-SiO_2 and nano-$CaCO_3$ on properties of ultra-high performance cementitious composites. *Journal of Southeast University (Natural ence Edition)* 45(2):393-398, DOI: 10.3969/j.issn.1001-0505.2015.02.034
Roy K, Debnath SC, Raengthon N, Potiyaraj P (2019) Understanding the reinforcing efficiency of waste eggshell-derived nano calcium carbonate in natural rubber composites with maleated natural rubber as compatibilizer. *Polymer Engineering & Science* 59(7):1428-1436, DOI: 10.1002/pen.25127
Sacerdote L, Tamborrino M, Zucca C (2016) First passage times of two-dimensional correlated processes: Analytical results for the Wiener process and a numerical method for diffusion processes. *Journal of Computational and Applied Mathematics* 296:275-292, DOI: 10.1016/j.cam.2015.09.033
Sato T, Beaudoin JJ (2011) Effect of nano-$CaCO_3$ on hydration of cement containing supplementary cementitious materials. *Advances in Cement Research* 23(1):33-43, DOI: 10.1680/adcr.9.00016
Sato T, Diallo F (2010) Seeding effect of nano-$CaCO_3$ on the hydration of tricalcium silicate. *Transportation Research Record: Journal of the Transportation Research Board* 2141(1):61-67, DOI: 10.3141/2141-11
Shaikh FUA, Supit SWM (2014) Mechanical and durability properties of high volume fly ash (HVFA) concrete containing calcium carbonate ($CaCO_3$) nanoparticles. *Construction and Building Materials* 70:309-321, DOI: 10.1016/j.conbuildmat.2014.07.099
Shaikh FUA, Supit SWM (2015) Chloride induced corrosion durability of high volume fly ash concretes containing nano particles. *Construction and Building Materials* 99:208-225, DOI: 10.1016/j.conbuildmat.2015.09.030
Suleiman AR, Soliman AM, Nehdi ML (2014) Effect of surface treatment on durability of concrete exposed to physical sulfate attack. *Construction and Building Materials* 73:674-681, DOI: 10.1016/j.conbuildmat.2014.10.006
Sun Y, Zhang P, Guo W, Bao J, Qu C (2020) Effect of nano-$CaCO_3$ on the mechanical properties and durability of concrete incorporating Fly Ash. *Advances in Materials Science and Engineering* 2020:1-10, DOI: 10.1155/2020/7365862
Tian B, Cohen MD (2000) Does gypsum formation during sulfate attack on concrete lead to expansion? *Cement and Concrete Research* 30(1):117-123, DOI: 10.1016/S0008-8846(99)00211-2
Uthaman S, George RP, Vishwakarma V, Harilal M, Philip J (2019) Enhanced seawater corrosion resistance of reinforcement in nanophase modified fly ash concrete. *Construction and Building Materials* 221:232-243, DOI: 10.1016/j.conbuildmat.2019.06.070
Wang H, Liao H, Ma X (2022) Stochastic multi-phase modeling and health assessment for systems based on degradation branching processes. *Reliability Engineering & System Safety* 222:108412, DOI: 10.1016/j.ress.2022.108412
Wu Z, Khayat KH, Shi C, Tutikian BF, Chen Q (2021) Mechanisms underlying the strength enhancement of UHPC modified with nano-SiO_2 and nano-$CaCO_3$. *Cement and Concrete Composites* 119:103992, DOI: 10.1016/j.cemconcomp.2021.103992
Wu Z, Shi C, Khayat KH (2018) Multi-scale investigation of microstructure, fiber pullout behavior, and mechanical properties of ultra-high performance concrete with nano-$CaCO_3$ particles. *Cement and Concrete Composites* 86:255-265, DOI: 10.1016/j.cemconcomp.2017.11.014
Wu Z, Shi C, Khayat KH, Wan S (2016) Effects of different nanomaterials on hardening and performance of ultra-high strength concrete (UHSC). *Cement and Concrete Composites* 70:24-34, DOI: 10.1016/j.cemconcomp.2016.03.003
Yeşilmen S, Al-Najjar Y, Balav MH, Şahmaran M, Yıldırım G, Lachemi M (2015) Nano-modification to improve the ductility of cementitious composites. *Cement and Concrete Research* 76:170-179, DOI: 10.1016/j.cemconres.2015.05.026
Yu H, Li JM, Xin H (2013) Study on corrosion resistant performance of sulfoaluminate cement. *Advanced Materials Research* 710:362-366, DOI: 10.4028/www.scientific.net/AMR.710.362
Zheng M (2010) Salt lake resources and eco-environment in China. *Acta Geologica Sinica* 84:1613-1622, DOI: 10.19762/j.cnki.dizhixuebao.2010.11.007 (in Chinese)
Zhou gang Li S, Wang Z, Wang C (2011) Investigation and analysis on corrosion situation of concrete in saline soil region. *Journal of Architecture and Civil Engineering* 28(4):121-126, DOI: 10.19815/j.jace.2011.04.019 (in Chinese)

Appendix

Table 7. Average Compressive Strength in the T Area of the Specimen (MPa)

Time	H0	H1	H2	H3	H4	H5
0 d	60.63	64.02	59.50	61.31	56.50	54.30
60 d	63.60	67.26	62.78	65.22	60.15	57.08
120 d	67.30	71.64	66.18	69.66	63.67	60.23
180 d	69.39	74.04	68.30	70.60	65.12	61.29
240 d	61.51	66.91	61.10	62.56	55.12	51.90
300 d	55.57	61.13	55.14	57.29	50.36	47.34
360 d	51.68	57.20	51.00	53.38	44.54	42.16

Table 8. Average Compressive Strength in the D Area of the Specimen (MPa)

Time	H0	H1	H2	H3	H4	H5
0 d	60.63	64.02	59.50	61.31	56.50	54.30
60 d	65.20	66.81	61.10	63.58	58.51	56.45
120 d	65.39	68.05	62.30	66.07	59.78	57.08
180 d	67.12	70.73	62.67	67.77	61.08	58.42
240 d	62.43	68.67	61.20	61.42	56.29	53.97
300 d	58.34	64.54	58.15	59.04	54.28	51.59
360 d	54.94	60.72	54.30	55.30	48.35	43.82

Table 9. Average Flexural Strength of the Specimen (MPa)

Time	H0	H1	H2	H3	H4	H5
0 d	6.61	7.58	7.23	6.89	6.55	6.23
60 d	6.84	8.46	7.73	7.26	6.72	6.40
120 d	7.10	8.89	8.09	7.47	6.95	6.65
180 d	7.81	9.69	8.27	7.81	7.32	6.82
240 d	6.08	7.62	6.82	6.54	5.99	5.48
300 d	5.90	7.41	6.60	6.19	5.78	5.31
360 d	5.37	6.78	6.10	5.75	5.18	4.81

Table 10. Average Mass of the Specimen (g)

Time	H0	H1	H2	H3	H4	H5
0 d	10125	10130	10050	10115	10225	10165
60 d	10130	10145	10060	10125	10230	10170
120 d	10135	10155	10065	10130	10235	10175
180 d	10155	10180	10080	10145	10250	10190
240 d	10135	10165	10060	10120	10225	10160
300 d	10115	10150	10040	10095	10195	10120
360 d	10085	10125	10010	10060	10155	10080

Table 11. Average Ultrasonic Velocity in the T Area of the Specimen (km/s)

Time	H0	H1	H2	H3	H4	H5
0 d	4.173	4.255	4.170	4.130	4.098	4.082
60 d	4.261	4.440	4.258	4.202	4.140	4.105
120 d	4.450	4.596	4.453	4.309	4.169	4.124
180 d	4.552	4.749	4.562	4.405	4.329	4.291
240 d	4.258	4.440	4.273	4.271	4.147	4.105
300 d	4.156	4.340	4.173	4.173	4.052	4.007
360 d	3.956	4.136	3.953	3.816	3.737	3.576

Table 12. Average Ultrasonic Velocity in the M Area of the Specimen (km/s)

Time	H0	H1	H2	H3	H4	H5
0 d	4.173	4.255	4.170	4.130	4.098	4.082
60 d	4.264	4.493	4.303	4.174	4.141	4.125
120 d	4.362	4.595	4.403	4.271	4.238	4.183
180 d	4.561	4.749	4.562	4.329	4.377	4.263
240 d	4.117	4.440	4.273	4.045	3.997	3.962
300 d	3.933	4.289	4.073	3.834	3.756	3.693
360 d	3.629	4.033	3.703	3.591	3.419	3.214

Table 13. Average Ultrasonic Velocity in the D Area of the Specimen (km/s)

Time	H0	H1	H2	H3	H4	H5
0 d	4.173	4.255	4.170	4.130	4.098	4.082
60 d	4.241	4.400	4.248	4.212	4.180	4.134
120 d	4.456	4.600	4.403	4.361	4.229	4.173
180 d	4.607	4.762	4.623	4.510	4.376	4.261
240 d	4.261	4.404	4.193	4.143	4.109	4.084
300 d	4.106	4.250	4.093	3.994	3.934	3.869
360 d	3.731	4.050	3.822	3.693	3.600	3.460